 CMES, vol.73, no.2, pp.183-207, 2011

Application of Polygonal Finite Elements to Two-Dimensional Mechanical and Electro-Mechanically Coupled Problems

K. Jayabal[1] **and A. Menzel**[1,2]

Abstract: Naturally evolving Voronoi discretisation of two-dimensional plane domains renders representative microstructures that turn out to be useful for the modelling and simulation of polycrystalline materials. Hybrid finite element approaches are employed on such polygonal discretisations to solve, for instance, mechanical and electromechanical problems within a finite element context. In view of solving mechanical problems, varying order of polynomial functions are suggested in the literature to sufficiently approximate stresses within the polygonal finite elements. These are, in addition to the order of the approximation functions for the displacements, characterised by the number of edges in the polygonal elements. It appears, as demonstrated in this work, that the naturally evolving Voronoi discretisations exhibit a specific property when combined with a hybrid polygonal finite element approach. This property allows the choice of stress approximating functions in polygonal finite elements to be based only on the order of the displacement approximating functions regardless of the number of edges in the element. Such a relation also appears to hold in coupled electromechanical problems between the approximating functions for the electric displacements and the electric potential. The realisation of such a property is demonstrated through several standard numerical examples and also with an application on a representative piezoceramic microstructure.

Keywords: Polygonal finite element, Voronoi discretisations, approximation functions, electromechanically coupled problems, piezoceramics.

1 Introduction

Discretisation of the domain of interest is one of the preliminary steps for finite element simulations to solve complex boundary value problems. A great deal of

[1] Institute of Mechanics, TU Dortmund, Germany
[2] Division of Solid Mechanics, Lund University, Sweden

effort has been directed towards meshing algorithms in accomplishing such partitions. Within standard finite element approaches applied to the discretisation and modelling of polycrystalline microstructures, for instance piezoceramics, the grain structure may be represented either by, for example, rectangular elements (Kamlah, Liskowsky, McMeeking, and Balke, 2005) or hexagonal elements (Haug, Huber, Onck, and Van der Giessen, 2007; Kim and Jiang, 2002) with each element representing an individual grain. Randomly oriented crystal axes within the finite elements, or rather grains, together with the corresponding material properties realise the locally anisotropic nature of the polycrystalline structure. The grain to grain interaction effects, which are explicitly taken into account by the finite element formulation, depend on how the material properties vary between one element and its neighbouring elements. The potential deficit of restricted grain shapes can be relatively overcome by considering a Voronoi-cell-based discretisation of the polycrystalline microstructure. Voronoi discretisation is widely considered to be one of the most fundamental geometric structures associated with a discrete set of points (Aurenhammer, 1991). Given a set of isolated points in a plane, the associated Voronoi diagram partitions the plane according to the nearest neighbour rule. Each of the given points is associated with the region of the plane closest to it, called its Voronoi cell. By this Voronoi discretisation, a representative microstructure of a polycrystalline material is constructed by the underlying Dirichlet tessellation so that each irregular polygon, i.e. the Voronoi cell, represents a single grain.

With this Voronoi discretisation in hand, one way to proceed further towards the micromechanical modelling of polycrystalline materials is to subdiscretise the individual polygons or rather grains by means of several standard quadrilateral or triangular elements. In fact, this approach might turn out to be computationally rather expensive especially in view of iterative finite element formulations for nonlinear problems. Alternatively, one may apply a Voronoi-cell-based finite element method (Ghosh and Mallett, 1994; Ghosh and Moorthy, 1995) which is also referred to as the polygonal finite element method (PolyFEM). Such a hybrid formulation, as proposed earlier by Pian (1964), allows to avoid further subdiscretisation of a crystal grain, the geometry of which is here assumed to be represented by a Voronoi polygon. An application of this framework to the simulation of the nonlinear behaviour of ferroelectrics has been investigated by Sze and Sheng (2005). While solving mechanical boundary value problems, the PolyFEM approximates stresses within polygonal finite elements in addition to defining mechanical displacements as degrees of freedom. In the case of coupled electromechanical problems, in addition to the stresses and displacements, the electric displacements and the electric potential are also approximated, respectively, within the element and along the element boundary. Upon application of the PolyFEM, it is suggested to employ varying

order polynomial approximation functions for stresses (Ghosh and Mallett, 1994) and electric displacements (Sze and Sheng, 2005) based on the number of edges in the polygonal element in order to avoid rank deficiency by the element stiffness matrices. For instance, when the displacement is defined by a linear polynomial function along the element edges, a constant and a fourth order polynomial functions are introduced for stress approximations in polygonal finite elements with three and eleven edges respectively. On the contrary, several simulations in the present work show that Voronoi-polygon-based meshes seem to provide a certain facilitation on the selection of approximation functions for stresses in the PolyFEM. Accordingly, the approximation function for stresses in a polygonal element may be chosen based only on the order of polynomial function defining the displacements along element edges without paying any attention to the number of edges in the element. In the case of electromechanically coupled problems, the above mentioned relation also holds between the approximation functions of the electric displacements and the electric potential.

This paper is arranged as follows: section 2 reviews the formulation of the PolyFEM for coupled electromechanical problems which can easily be reduced to purely mechanical or electrical cases. With numerical examples, section 3 and 4 discuss on the selection of the order of polynomial approximation functions for the stresses and the electric displacements within the elements based on the approximation functions, defining the displacements and the electric potential along the element edges respectively. Application of the PolyFEM to a poled piezoceramic microstructure is presented in section 5 and the paper closes with a brief summary in section 6.

2 PolyFEM for electromechanical problems

Unlike for standard isoparametric finite element formulations, within the PolyFEM the displacements and the electric potential are introduced only along the interelement boundaries. On the other hand, the corresponding flux terms, i.e. the stresses and the electric displacements, are defined in the interior of each polygonal element. The construction of the element stiffness matrix for the PolyFEM will briefly be reviewed for electromechanically coupled problems in this section. For more details, see Sze and Sheng (2005). By removing either the electrical or mechanical contributions, the following derivation reduces to purely mechanical (Ghosh and Mallett, 1994) or electrical problems, respectively.

2.1 Basic equations

Electromechanical equilibrium, or rather the local balance of linear momentum together with the local form of Gauss' law, of a piezoelectric body under static

conditions allows representation as,

$$\nabla \cdot \boldsymbol{\sigma} + \boldsymbol{b} = \boldsymbol{0}, \qquad \nabla \cdot \boldsymbol{D} - q = 0, \tag{1}$$

where $\boldsymbol{\sigma}$ and $\boldsymbol{b}$ denote the stresses and volume forces and $\boldsymbol{D}$ and q refer to the electric displacements and volume electric charge density. As this work proceeds, $\boldsymbol{b}$ and q are considered negligible. Assuming that the strains $\boldsymbol{\varepsilon}$ remain sufficiently small, suitable deformation measures are introduced based on the displacement field $\boldsymbol{u}$, and the electric field $\boldsymbol{E}$ is derived from the electric potential ϕ, i.e.

$$\boldsymbol{\varepsilon} = \tfrac{1}{2}\left[\nabla \boldsymbol{u} + \nabla^{\mathrm{t}} \boldsymbol{u}\right] = \nabla^{\mathrm{sym}} \boldsymbol{u}, \qquad \boldsymbol{E} = -\nabla \phi\,. \tag{2}$$

The linear constitutive relations of coupled electromechanical problems, for instance in piezoelectric materials, can be expressed in matrix or rather Voigt (index v) notation as

$$\begin{bmatrix} \boldsymbol{\sigma}_{\mathrm{v}} \\ \boldsymbol{D} \end{bmatrix} = \begin{bmatrix} \boldsymbol{s}_{\mathrm{v}} & \boldsymbol{e}_{\mathrm{v}}^{\mathrm{t}} \\ \boldsymbol{e}_{\mathrm{v}} & -\boldsymbol{h} \end{bmatrix} \cdot \begin{bmatrix} \boldsymbol{\varepsilon}_{\mathrm{v}} \\ -\boldsymbol{E} \end{bmatrix} = \boldsymbol{S} \cdot \begin{bmatrix} \boldsymbol{\varepsilon}_{\mathrm{v}} \\ -\boldsymbol{E} \end{bmatrix}, \tag{3}$$

wherein $\boldsymbol{s}$, $\boldsymbol{e}$, $\boldsymbol{h}$ denote the elastic stiffness, piezoelectric and dielectric tensors respectively, and $\boldsymbol{S}$ refers to the electromechanical stiffness matrix; see e.g. Nye (1985). Assuming the body forces and volume charge densities to vanish and considering a quasi-static case, the principle of electromechanical virtual work can be represented as

$$\int_{\mathscr{B}} \boldsymbol{\sigma} : \delta\boldsymbol{\varepsilon} - \boldsymbol{D} \cdot \delta \boldsymbol{E} \, \mathrm{d}v - \int_{\partial \mathscr{B}_t} \bar{\boldsymbol{t}} \cdot \delta \boldsymbol{u} \, \mathrm{d}a + \int_{\partial \mathscr{B}_w} \bar{w}\, \delta\phi \, \mathrm{d}a = 0\,, \tag{4}$$

with $\mathscr{B}$ denoting the configuration of the body considered. The boundary is characterised by $\partial\mathscr{B}_t$ and $\partial\mathscr{B}_w$ with prescribed surface traction $\bar{\boldsymbol{t}}$ and surface charge density $\bar{w}$; see Landis (2002) among others.

2.2 Approximation based on PolyFEM

After discretising the considered plane area by means of Voronoi-discretisation-based-polygonal finite elements $\mathscr{B}^e$ and by application of the divergence theorem in combination with the use of the electromechanical fluxes $\boldsymbol{\sigma}$ and $\boldsymbol{D}$ being in equilibrium, Eq. (4) can be rewritten as

$$\begin{aligned} \Pi \;=\; \sum_e \int_{\partial\mathscr{B}^e} \begin{bmatrix} \boldsymbol{\sigma}_{\mathrm{v}} \cdot \boldsymbol{n} \\ \boldsymbol{D} \cdot \boldsymbol{n} \end{bmatrix} \cdot \begin{bmatrix} \boldsymbol{u} \\ \phi \end{bmatrix} \mathrm{d}a - \int_{\mathscr{B}^e} \frac{1}{2} \begin{bmatrix} \boldsymbol{\sigma}_{\mathrm{v}} \\ \boldsymbol{D} \end{bmatrix} \cdot \boldsymbol{S}^{-1} \cdot \begin{bmatrix} \boldsymbol{\sigma}_{\mathrm{v}} \\ \boldsymbol{D} \end{bmatrix} \mathrm{d}v \\ - \int_{\partial\mathscr{B}_t^e} \bar{\boldsymbol{t}} \cdot \boldsymbol{u} \, \mathrm{d}a + \int_{\partial\mathscr{B}_w^e} \bar{w}\, \phi \, \mathrm{d}a\,, \end{aligned} \tag{5}$$

where $\boldsymbol{n}$ denotes the outward unit normal vector of element edges and Π is often referred to as Hellinger-Reissner functional. As seen in Eq. (5), solely $\boldsymbol{\sigma}$ and $\boldsymbol{D}$ need to be determined within the element ($\mathscr{B}^e$), whereas $\boldsymbol{u}$ and ϕ have to be specified only along the element boundary ($\partial\mathscr{B}^e$) satisfying continuity conditions. These properties allow to introduce any number of element edges for a polygonal finite element. The polynomial approximation of the flux terms is chosen such that the equilibrium conditions are satified. In this context, using an element-related matrix-vector-type notation results in the representation

$$\begin{bmatrix} \boldsymbol{\sigma}_{\mathrm{v}} \\ \boldsymbol{D} \end{bmatrix} \approx \begin{bmatrix} \boldsymbol{M}_\sigma & \boldsymbol{0} \\ \boldsymbol{0} & \boldsymbol{M}_D \end{bmatrix} \cdot \begin{bmatrix} \boldsymbol{\beta}_\sigma \\ \boldsymbol{\beta}_D \end{bmatrix} = \boldsymbol{M} \cdot \boldsymbol{\beta}_e \,, \tag{6a}$$

$$\begin{bmatrix} \boldsymbol{u} \\ \phi \end{bmatrix} \approx \begin{bmatrix} \boldsymbol{N}_u & \boldsymbol{0} \\ \boldsymbol{0} & \boldsymbol{N}_\phi \end{bmatrix} \cdot \begin{bmatrix} \boldsymbol{q}_u \\ \boldsymbol{q}_\phi \end{bmatrix} = \boldsymbol{N} \cdot \boldsymbol{q}_e \,, \tag{6b}$$

where $\boldsymbol{\beta}_e$ and $\boldsymbol{q}_e$ are vectorial quantities collecting the coefficients for the approximation of the fluxes and the nodal degrees of freedom on the element level. The matrix-entries in $\boldsymbol{M}$ are polynomial functions in element coordinates, whereas the nodal interpolation functions $\boldsymbol{N}$ are defined by the boundary coordinates $\boldsymbol{q}_e$. Hence, it turns out that linear shape functions are sufficient for plane problems to interpolate $\boldsymbol{q}_e$ as they are defined only along the element edges. The comination of Eq. (5) and (6) then yields the functional Π to take the more compact form

$$\Pi = \sum_e \boldsymbol{\beta}_e \cdot \boldsymbol{G}_e \cdot \boldsymbol{q}_e - \frac{1}{2} \boldsymbol{\beta}_e \cdot \boldsymbol{J}_e \cdot \boldsymbol{\beta}_e - \boldsymbol{q}_e \cdot \boldsymbol{f}_e \,, \tag{7}$$

where

$$\boldsymbol{G}_e = \int_{\partial\mathscr{B}^e} \boldsymbol{M}^{\mathrm{t}} \cdot [\boldsymbol{n} \cdot \boldsymbol{N}] \, \mathrm{d}a \,, \qquad \boldsymbol{J}_e = \int_{\mathscr{B}^e} \boldsymbol{M}^{\mathrm{t}} \cdot \boldsymbol{S}^{-1} \cdot \boldsymbol{M} \, \mathrm{d}v \,, \tag{8a}$$

$$\boldsymbol{f}_e = \begin{bmatrix} \int_{\partial\mathscr{B}_t^e} \boldsymbol{N}_u \cdot \bar{\boldsymbol{t}} \, \mathrm{d}a \\ -\int_{\partial\mathscr{B}_w^e} \boldsymbol{N}_\phi \, \bar{w} \, \mathrm{d}a \end{bmatrix} . \tag{8b}$$

By making use of Eq. (7), the stationary point of Π with respect to $\boldsymbol{\beta}_e$—such that $\partial_{\boldsymbol{\beta}_e}\Pi = \boldsymbol{0}$—results in $\boldsymbol{\beta}_e = \boldsymbol{J}_e^{-1} \cdot \boldsymbol{G}_e \cdot \boldsymbol{q}_e$. Next, substituting this relation for $\boldsymbol{\beta}_e$ into Eq. (7) ends up with

$$\Pi = \sum_e \frac{1}{2} \boldsymbol{q}_e \cdot \boldsymbol{G}_e^{\mathrm{t}} \cdot \boldsymbol{J}_e^{-1} \cdot \boldsymbol{G}_e \cdot \boldsymbol{q}_e - \boldsymbol{q}_e \cdot \boldsymbol{f}_e \,. \tag{9}$$

Moreover, the stationary point of Π with respect to $\boldsymbol{q}_e$—such that $\partial_{\boldsymbol{q}_e}\Pi = \mathbf{0}$—results in

$$\sum_e \boldsymbol{G}_e^{\mathrm{t}} \cdot \boldsymbol{J}_e^{-1} \cdot \boldsymbol{G}_e \cdot \boldsymbol{q}_e = \sum_e \boldsymbol{f}_e \,, \tag{10}$$

which, by analogy with standard linear finite element represenrtations, can be written as $\sum_e \boldsymbol{K}_e \cdot \boldsymbol{q}_e = \sum_e \boldsymbol{f}_e$ with $\boldsymbol{K}_e = \boldsymbol{G}_e^{\mathrm{t}} \cdot \boldsymbol{J}_e^{-1} \cdot \boldsymbol{G}_e$. After evaluating the nodal electromechanical degrees of freedom $\boldsymbol{q}_e$, the electromechanical flux coefficients of the element $\boldsymbol{\beta}_e$ can be determined. The element electromechanical fluxes can then be obtained from Eq. (6a) which, in turn, will provide $\boldsymbol{\varepsilon}$ and $\boldsymbol{E}$ from Eq. (3).

3 Application of PolyFEM to mechanical problems

The PolyFEM formulation derived in section 2 for coupled electromechanical cases will reduce to purely mechanical problems by removing the electrical and piezoelectric terms. Under such conditions, Eqs. (3), (6) and (8) turn out to be,

$$\boldsymbol{\sigma}_{\mathrm{v}} = \boldsymbol{s}_{\mathrm{v}} \cdot \boldsymbol{\varepsilon}_{\mathrm{v}} \;= \boldsymbol{S} \cdot \boldsymbol{\varepsilon}_{\mathrm{v}} \approx \boldsymbol{M}_\sigma \cdot \boldsymbol{\beta}_\sigma = \boldsymbol{M} \cdot \boldsymbol{\beta}_e \,, \tag{11}$$

$$\boldsymbol{u} \;\approx \boldsymbol{N}_u \cdot \boldsymbol{q}_u = \boldsymbol{N} \cdot \boldsymbol{q}_e \,, \tag{12}$$

$$\boldsymbol{G}_e = \int_{\partial\mathscr{B}^e} \boldsymbol{M}_\sigma^{\mathrm{t}} \cdot [\boldsymbol{n} \cdot \boldsymbol{N}_u] \,\mathrm{d}a \,, \quad \boldsymbol{J}_e = \int_{\mathscr{B}^e} \boldsymbol{M}_\sigma^{\mathrm{t}} \cdot \boldsymbol{s}_{\mathrm{v}} \cdot \boldsymbol{M}_\sigma \,\mathrm{d}v \,, \quad \boldsymbol{f}_e = \int_{\partial\mathscr{B}_t^e} \boldsymbol{N}_u \cdot \bar{\boldsymbol{t}} \,\mathrm{d}a \,. \tag{13}$$

For the approximation of stress fields in Eq. (11), the Airy stress function can be employed to generate polynomial functions satisfying mechanical equilibrium conditions in polygonal elements. To secure the invariance of the approximation of the stresses, the assumed polynomial functions should be considered up to certain polynomial orders. For two-dimensional plane problems, they can be represented as functions of coordinates, say, x and z, as

$$\boldsymbol{M}_\sigma^0 = \begin{bmatrix} 0 & 0 & 1 \\ 1 & 0 & 0 \\ 0 & 1 & 0 \end{bmatrix}, \qquad \boldsymbol{M}_\sigma^1 = \begin{bmatrix} \boldsymbol{M}_\sigma^0 & \begin{matrix} 0 & 0 \\ x & z \\ 0 & -x \end{matrix} & \begin{matrix} x & z \\ 0 & 0 \\ -z & 0 \end{matrix} \end{bmatrix}, \tag{14a}$$

$$\boldsymbol{M}_\sigma^2 = \begin{bmatrix} \boldsymbol{M}_\sigma^1 & \begin{matrix} 0 & 0 & x^2 \\ x^2 & 2xz & z^2 \\ 0 & -x^2 & -2xz \end{matrix} & \begin{matrix} 2xz & z^2 \\ 0 & 0 \\ -z^2 & 0 \end{matrix} \end{bmatrix}, \tag{14b}$$

$$\boldsymbol{M}_\sigma^3 = \begin{bmatrix} \boldsymbol{M}_\sigma^2 & \begin{matrix} 0 & 0 & x^3 \\ x^3 & 3x^2z & 3xz^2 \\ 0 & -x^3 & -3x^2z \end{matrix} & \begin{matrix} 3x^2z & 3xz^2 & z^3 \\ z^3 & 0 & 0 \\ -3xz^2 & -z^3 & 0 \end{matrix} \end{bmatrix}, \tag{14c}$$

Table 1: The order of polynomial function $\boldsymbol{M}_\sigma$ suggested for approximating the stresses based on the number of edges in the polygonal element(Ghosh and Mallett, 1994).

approximation of	number of edges in polygonal element									
displacements $\boldsymbol{u}$	3	4	5	6	7	8	9	10	11	12
linear	0	1	1	2	2	3	3	3	4	4
quadratic	2	3	3	4	4	5	5	6	6	7
cubic	3	4	5	5	6	7	7	8	8	9

where the superscripts indicate the order of polynomial functions that approximate the stress fields in polygonal elements. Further higher orders of $\boldsymbol{M}_\sigma$ can be constructed by adopting the same procedure. It is clear from Eqs. (12) and (13) that the displacements need to be defined only along the element boundaries. Hence, even a linear polynomial function in terms of the edge coordinates would suffice to define displacements along the element edge–here a line–whereas higher order approximations may also be considered. The element stiffness matrix $\boldsymbol{K}_e$ should satisfy the following necessary but not sufficient condition to be rank sufficient,

$$m \geq i * d - r \,, \tag{15}$$

where m, i, d and r refer to, respectively, the rank of the element stiffness matrix, number of nodes in the polygonal element, degree of freedom per node and the number of rigid body modes of the element. For plane problems, d and r become two and three denoting two displacements per node and three rigid body motions of the element – two translations and one rotation. Since a polygonal discretisation of plane domains results in elements with varying edges, for instance, three to eleven, the size of individual element stiffness matrices are not the same. Further elaborating the elment stiffness matrix and (13) reveals that the rank of $\boldsymbol{K}_e$ not only depends on the number of nodes in the polygonal element but also on the choice of stress approximation functions or, in other words, on the number of columns in $\boldsymbol{M}_\sigma$. Hence, consistent with Eq. (15) and also for the completeness of polynomial approximation functions, it has been suggested to use different higher order representations of $\boldsymbol{M}_\sigma$ for stresses to make every individual $\boldsymbol{K}_e$ rank sufficient (Ghosh and Mallett, 1994). Accordingly, Tab. 1 indicates the order of $\boldsymbol{M}_\sigma$ to be considered based on the number of edges in the polygonal element and also on the order of the approximation functions for the displacements. This way, the global stiffness matrix turns out to be free of any singularities and can straightforwardly be inverted. On the other hand, it is evident that the use of higher order polynomial functions leads to considerable computational cost. For instance, let us consider a

case wherein a linear polynomial function approximates displacements along the element edges. According to Tab. 1, polynomial approximation $\boldsymbol{M}_\sigma$ of first and fourth order has to be applied to the stress field for polygonal elements with four and eleven edges. The order of $\boldsymbol{M}_\sigma$ for the same elements will increase to four and eight when cubic approximations are employed for the displacements. One may observe from Eq. (13) that the size of the matrices $\boldsymbol{G}_e$ and $\boldsymbol{J}_e$ and also the computational time to determine $\boldsymbol{K}_e$ increase with the order of polynomial approximation $\boldsymbol{M}_\sigma$ for the stresses. Hence, the use of higher order $\boldsymbol{M}_\sigma$ for PolyFEM leads to higher computational cost, especially when nonlinear problems are solved.

In this context, it is observed as the work proceeds that there appears to be a specific property associated with the Voronoi-based discretisation of plane domains. This property reveals that there is no necessity to make each and every individual $\boldsymbol{K}_e$ to be rank sufficient while applying PolyFEM to Voronoi based discretisations in order to render the global stiffness matrix, after enforcing the essential boundary conditions, rank sufficient. As a consequence, instead of choosing varying order of polynomial stress approximations for different polygonal elements, a common polynomial approximation can be employed in all polygonal elements. Furthermore, such a polynomial function can be selected only based on the order of the polynomial function defining the displacements along the element edges. For instance, while using linear approximation functions for $\boldsymbol{u}$, only $\boldsymbol{M}_\sigma^1$ needs to be employed in all polygonal elements in the Voronoi based mesh regardless of the number of edges in the element. Similarly, $\boldsymbol{M}_\sigma^2$ and $\boldsymbol{M}_\sigma^3$ would be adequate to define stresses in all polygonal elements when quadratic and cubic approximations are chosen for $\boldsymbol{u}$. Such a relation between the approximation functions of stresses and displacements allows the global stiffness matrix, although not all the individual $\boldsymbol{K}_e$, to always turn out rank sufficient after enforcing the essential boundary conditions. This specific behaviour of Voronoi based discretisation is demonstrated by some standard numerical examples in the following sections.

3.1 Numerical examples

A 1×1 mm^2 two-dimensional plane domain is discretised by Voronoi based polygons with the total number of elements chosen as 10, 50, 100, 200, 300 and 500. The number of edges in the polygonal elements is found to be varying from three to eleven. The Voronoi based mesh with 50 polygonal elements is shown in Fig. 1 where l and h denote the length and height of the discretised domain. In order to apply identical essential boundary conditions for all six types of discretisations, the node lying on the left boundary of the domain with its z coordinate closest to $\frac{1}{2}h$ was moved to the position $[0,\frac{1}{2}\mathrm{h}]$ for all polygonal meshes. Similarly, to facilitate the comparison of the simulated results with the exact solutions, the node lying on

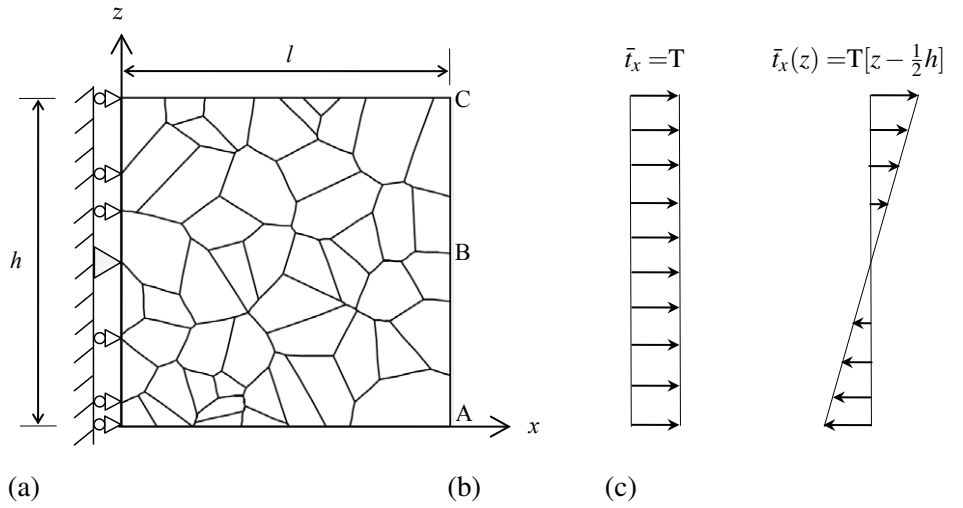

Figure 1: (a) Voronoi based discretisation of a plane domain with 50 polygonal elements and visualisation of the essential boundary conditions. Tractions enforced at $x = l$ for (b) tension and (c) pure bending.

the right boundary of the domain and z coordinate closest to $\frac{1}{2}h$ was moved to $[l, \frac{1}{2}h]$ for all polygonal meshes. Homogeneous and isotropic material properties are assigned to all the elements with a Young's modulus E of 30 GPa and a Poisson's ratio ν of 0.3.

3.1.1 Tension test

A simple tension test under plane strain conditions is considered. As homogeneous material properties are taken into account, the displacements should vary linearly in longitudinal and transverse directions and the stresses remain constant for the exact solutions. While applying PolyFEM, linear polynomial functions are employed to approximate the displacements along element edges. Instead of considering the different stress approximations as suggested in Tab. 1, only first order polynomial approximation, i.e., $\boldsymbol{M}_{\sigma}^{1}$ is used for all polygonal elements irrespective of the number of edges. The displacement and traction boundary conditions are applied as displayed in Fig. 1(a) and (b), i.e.

$$\begin{aligned} u_x &= 0 \quad \text{at} \quad x = 0\,, \\ u_z &= 0 \quad \text{at} \quad [x,z] = [0, \tfrac{1}{2}h]\,, \\ \bar{t}_x &= \mathrm{T} \quad \text{at} \quad x = l\,. \end{aligned} \tag{16}$$

Table 2: Comparison of the displacements (in μm) between the analytical and the PolyFEM solution for tension loading.

	u_x at A	u_z at A	u_x at B	u_z at B	u_x at C	u_z at C
analytical	0.6667	0.1	0.6667	0	0.6667	-0.1
PolyFEM	0.6667	0.1	0.6667	0	0.6667	-0.1

Use of $\boldsymbol{M}_{\sigma}^{1}$ for all the elements produced the element stiffness matrices of the polygonal elements with more than five edges to become rank deficient. However, the global stiffness matrix pertained to all six types of Voronoi based meshes turned out full rank after enforcing the essential boundary conditions. For illustrative purposes, the results based on the PolyFEM are compared with the analytical solutions at three points A, $[l,\, 0]$, and B, $[l,\, \frac{1}{2}h]$, as well as C, $[l,\, h]$, as represented with respect to the $x-z$ coordinates in Fig. 1(a). A comparison of the respective displacements at these points is presented in Tab. 2 for T = 20 MPa. Identical results are obtained while using varying order of stress approximations for different polygonal elements according to the Tab. 1 along with linear approximations of the displacements. Although the stresses are constant throughout the domain for this loading case, attempts to use a constant stress approximation $\boldsymbol{M}_{\sigma}^{0}$ in all elements caused the global stiffness matrix to suffer from rank deficiencies for all six meshes.

3.1.2 Bending test

A pure bending case is considered next to further elaborate the Voronoi based discretisations in combination with the PolyFEM. The essential boundary conditions from Eq. (16) are retained and tractions $\bar{t}_x(z) = \mathrm{T}[z-\frac{1}{2}h]$ are applied as shown in Fig. 1(c). While applying the PolyFEM, the displacements are approximated by quadratic polynomial functions along the element edges. Again, without adopting different higher polynomial stress approximations from Tab. 1 according to the number of element edges, only $\boldsymbol{M}_{\sigma}^{2}$ was used for all polygonal elements. For the bending case considered, the expressions for the analytical solution of the displacements can be derived based on the specified coordinate system as

$$u_x = \frac{1}{\mathsf{E}}\mathrm{T}x[z-\tfrac{1}{2}h]; \quad u_z = -\frac{1}{2\mathsf{E}}\mathrm{T}\left[\nu\,[z-\tfrac{1}{2}h]^2 + x^2\right]. \tag{17}$$

On analysing the rank of individual element stiffness matrices, all $\boldsymbol{K}_e$ except those of triangular elements, arise rank deficient as expected. For instance, refer to the Voronoi based discretisation with 10 polygonal elements in Fig. 2(a) wherein no triangular element is included. None of the individual element stiffness matrices turned out to be rank sufficient in that mesh for the present case considered. How-

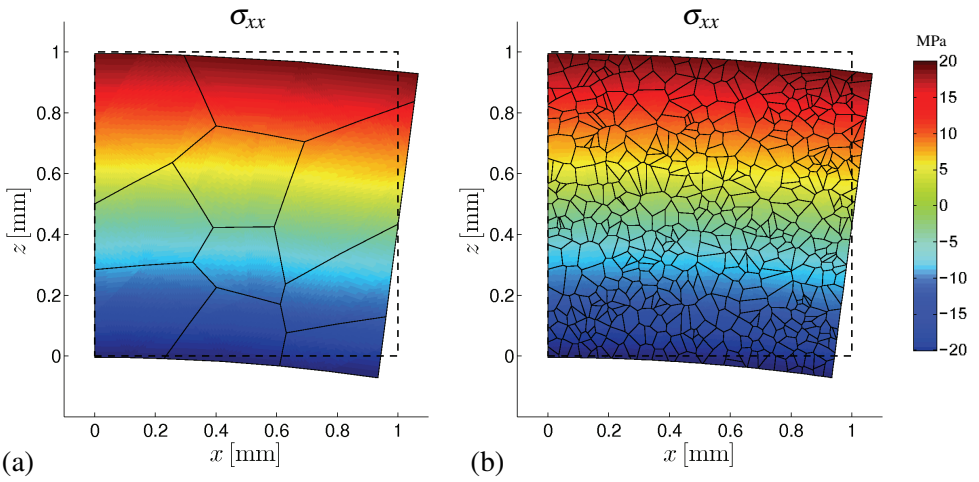

Figure 2: Visualisation of stress component σ_{xx} under pure bending for a discretisation with (a) 10 and (b) 500 polygonal elements. The undeformed domain boundary is shown in dashed lines whereas the deformed contour (here and in the following plots) is magnified by a factor of 100. While quadratic polynomial functions approximate the displacements along the element edges, $\boldsymbol{M}_\sigma^2$ is employed for the stress approximations for all polygonal finite elements, regardless of the number of edges.

ever, after the essential boundary conditions are enforced, the global stiffness matrix of that Voronoi mesh turns out to possess full rank which is the case for all other types of meshes as well. The PolyFEM produced exact solutions in combination with all types of Voronoi based meshes, and the displacements obtained at points A, B and C are compared with the analytical solutions (classical beam theory) in Tab. 3 for T = 20 MPa/mm. The distribution of the stress component along the x-axis, σ_{xx}, is visualised in Fig. 2 for discretisations with 10 and 500 polygonal meshes. Both types of meshes yield the same stress distribution across the domain. Use of only $\boldsymbol{M}_\sigma^0$ or $\boldsymbol{M}_\sigma^1$ in all polygonal elements caused the global stiffness matrix to fall short of rank in all six meshes. The introduction of stress approximations of polynomial order three in all polygonal elements apparently produced the exact solutions.

Table 3: Comparison of the displacements (in μm) between the analytical (classical beam theory) and the PolyFEM solution for pure bending.

	u_x at A	u_z at A	u_x at B	u_z at B	u_x at C	u_z at C
analytical	-0.3333	-0.3583	0	-0.3333	0.3333	-0.3583
PolyFEM	-0.3333	-0.3583	0	-0.3333	0.3333	-0.3583

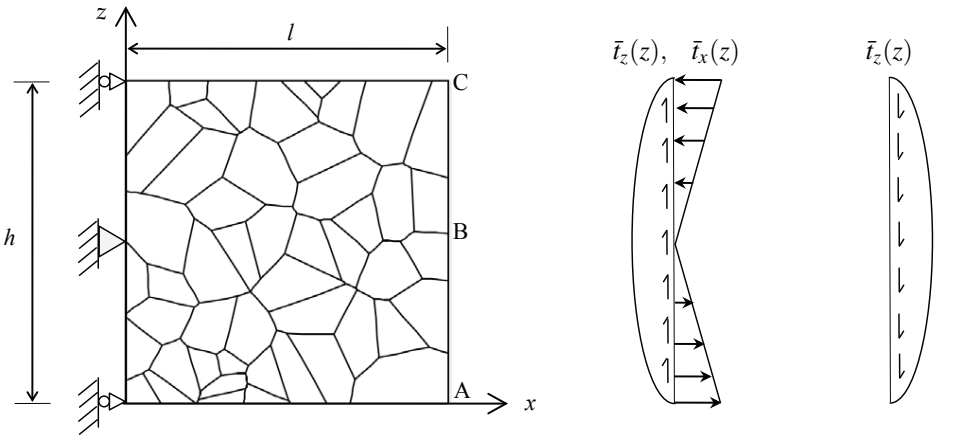

Figure 3: The boundary conditions for the loading case described in section 3.1.3 are displayed for (a) the displacements, and the tractions at (b) $x = 0$ and (c) at $x = l$.

3.1.3 Longitudinal and shear loading

Next, a more complex loading case is considered such that the displacements in the domain of interest vary cubically for the analytical solution. To accomplish this, a cantilever with a cross section of unit width is bent by a force applied at the free endings. The boundary conditions required to realize such a loading case, as specified in Fig. 3, can be expressed as,

$$\begin{aligned} u_x &= 0 \quad \text{at} \quad [x,z] = \{\,[0,0],\,[0,\tfrac{1}{2}h],\,[0,h]\,\}\,, \\ u_z &= 0 \quad \text{at} \quad [x,z] = [0,\tfrac{1}{2}h]\,, \end{aligned} \tag{18a}$$

$$\begin{aligned} \bar{t}_z &= -\frac{1}{h^3}\,6\,\mathrm{T}\,z\,[h-z] \quad \text{at} \quad x = 0 \text{ and } x = l\,, \\ \bar{t}_x &= -\frac{1}{h^3}\,6\,\mathrm{T}\,l\,[h-2z] \quad \text{at} \quad x = 0\,, \end{aligned} \tag{18b}$$

Table 4: Comparison of the displacements (in μm) between the analytical and the PolyFEM solution for the loading case represented in Fig. 3.

	u_x at A	u_z at A	u_x at B	u_z at B	u_x at C	u_z at C
analytical	-0.5	-1.125	0	-1.125	0.5	-1.125
PolyFEM	-0.5	-1.125	0	-1.125	0.5	-1.125

where T denotes the resultant force (per unit thickness) of traction $\bar{t}_z$ at the right (or left) boundary of the domain, i.e. $\int_0^h \bar{t}_z dz = \mathrm{T}$. The analytical solution for the displacement field for the problem at hand can be derived from Chapter 3, section 21, Timoshenko and Goodier (1970) by enforcing the displacement boundary conditions as described in Fig. 3(a) or as given in Eq. (18a)

$$u_x = \frac{1}{\mathsf{E}h^3}\mathrm{T}[h-2z]\,[3x(2l-x)-z(2+\nu)(h-z)]\,, \tag{19a}$$

$$u_z = \frac{2}{\mathsf{E}h^3}\mathrm{T}\big[(l-x)^3 - l^3 + 3\nu(l-x)(\tfrac{1}{2}h-z)^2 + x(3l^2+h^2+\tfrac{5}{4}\nu h^2)\big]\,. \tag{19b}$$

When solving the above mentioned boundary value problem with the PolyFEM, a cubic polynomial function is used to approximate the displacements along the element edges. According to Tab. 1, a fourth and an eighth order polynomial function would be required for approximating the stresses in polygonal finite elements, respectively, for four and eleven edges. On the contrary, $\boldsymbol{M}_\sigma^3$ is applied here for all polygonal elements and for all types of meshes. Recall that, apart from a very few elements, all other polygonal elements include between four and eleven edges. Hence, almost all individual $\boldsymbol{K}_e$ are rank deficient when making use of $\boldsymbol{M}_\sigma^3$. The global stiffness matrix, however, turns out to be rank sufficient for all types of Voronoi based meshes after incorporation of the essential boundary conditions. The use of the order of polynomial stress approximation below three in all polygonal elements along with cubic approximation of the displacements results in rank deficient global stiffness matrices in all six types of meshes. Application of stress approximations higher than three or according to Tab. 1 would also produce the exact solutions, though they are not investigated here, but obviously with higher computational cost. The PolyFEM produces exact solutions by employing only $\boldsymbol{M}_\sigma^3$ in all polygonal elements for all Voronoi based discretisations along with cubic approximation of the displacements. The obtained results are compared with analytical solutions in Tab. 4 for T = –5 kN/m. In addition, the distribution of the stress components σ_{xx} and τ_{xz} for a discretisation with 200 polygonal elements is presented in Fig. 4 which also reflects the exact distribution.

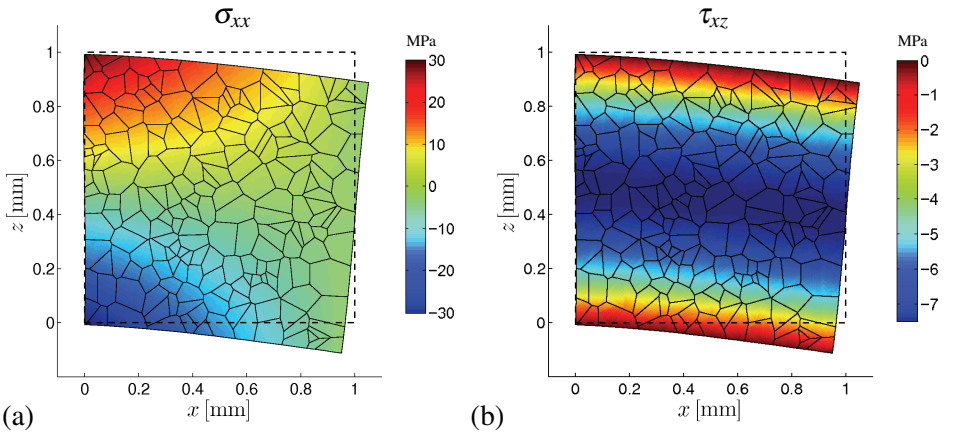

Figure 4: Distribution of stress components (a) σ_{xx} and (b) τ_{xz} for a discretisation with 200 polygonal finite elements for the loading case visualised in Fig. 3. While cubic polynomial function approximates the displacements along the element edges, $\boldsymbol{M}_{\sigma}^{3}$ is employed for the stress approximation for all polygonal elements.

3.1.4 A brief summary

The simulations and comparisons suggest that there is no necessity to make each and every individual element stiffness matrix to be rank sufficient while applying the PolyFEM on random Voronoi based discretisations to solve mechanical boundary value problems. Hence, varying higher order stress approximations are not required as given in Tab. 1 to approximate the stresses in polygonal finite elements with different number of edges. Instead, one needs to select the same order of stress approximation function in all polygonal elements based on the order of the approximation function for displacements along the element edges. Together with the use of appropriate integration rules, this renders the global stiffness matrix to be of full rank once the essential boundary conditions are incorporated. It is to be emphasised that the above mentioned property was studied only for specific discretisations based on random Voronoi generated tessellation. In general, this would not hold for special types of Voronoi discretisations where the mesh consists of repeated regular polygonal elements. For instance, if a plane domain is discretised by repeated square or rectangular elements, the above realisation does not hold – i.e., when using $\boldsymbol{M}_{\sigma}^{2}$ or $\boldsymbol{M}_{\sigma}^{3}$ for all elements in the mesh together with

employing quadratic or cubic polynomial approximations for $\boldsymbol{u}$. This could result in rank deficient global stiffness matrices. In summary, for Voronoi-based meshes not randomly generated, one may have to choose the order of $\boldsymbol{M}_\sigma$ according to Tab. 1.

The observations made above on the usage of interpolation functions for stresses in the context of the PolyFEM with Voronoi-based discretisations is here investigated to solve linear problems. Note that the global degrees of freedom (displacements) are approximated along the element edges while the flux terms (stresses) are interpolated within the element domain. If attempts are made to solve problems with constraints, for instance the analysis of incompressible media, one may have to take into account the ellipticity requirement and the Ladyzhenskaya-Babuska-Brezzi(LBB) condition; see Oden and Carey (1983); Brezzi and Fortin (1991); Braess (2001). This would ensure whether the polynomial shape functions used for the approximated fields provide stable elements and convergent solutions for such saddle point problems.

4 Application of PolyFEM to coupled electromechanical problems

The formulation discussed in section 3 holds in complete for electromechanically coupled problems and the electric and piezoelectric terms are now retained from section 2. Similar to the derivation of stress approximation functions, the polynomial functions of different orders satisfying electric equilibrium conditions can be derived from a potential function to approximate the electric displacements in the polygonal elements; see Sze and Sheng (2005). These polynomial approximations for the electric displacement, $\boldsymbol{M}_D$, should be taken up to certain complete polynomial orders to secure invariance. In the case of two-dimensional problems specified in the $x-z$ coordinate system, they take the form

$$\boldsymbol{M}_D^0 = \begin{bmatrix} 0 & 1 \\ 1 & 0 \end{bmatrix}, \qquad \boldsymbol{M}_D^1 = \begin{bmatrix} \boldsymbol{M}_D^0 & \begin{matrix} 0 \\ x \end{matrix} & \begin{matrix} x \\ -z \end{matrix} & \begin{matrix} z \\ 0 \end{matrix} \end{bmatrix}, \tag{20a}$$

$$\boldsymbol{M}_D^2 = \begin{bmatrix} \boldsymbol{M}_D^1 & \begin{matrix} 0 \\ x^2 \end{matrix} & \begin{matrix} x^2 \\ -2xz \end{matrix} & \begin{matrix} 2xz \\ -z^2 \end{matrix} & \begin{matrix} z^2 \\ 0 \end{matrix} \end{bmatrix}, \tag{20b}$$

$$\boldsymbol{M}_D^3 = \begin{bmatrix} \boldsymbol{M}_D^2 & \begin{matrix} 0 \\ x^3 \end{matrix} & \begin{matrix} x^3 \\ -3x^2z \end{matrix} & \begin{matrix} x^2z \\ -xz^2 \end{matrix} & \begin{matrix} 3xz^2 \\ -z^3 \end{matrix} & \begin{matrix} z^3 \\ 0 \end{matrix} \end{bmatrix}, \tag{20c}$$

where the superscripts of $\boldsymbol{M}_D$ denote the order of approximation functions of the electric displacements $\boldsymbol{D}$. Further higher order approximation functions can also be constructed by adopting the same procedure. As seen in Eq. (5), the electric potential ϕ needs to be defined only along the element boundary like the displacements

Table 5: The order of polynomial function $\boldsymbol{M}_D$ suggested for approximating the electric displacements based on the number of edges in the polygonal finite element(Sze and Sheng, 2005).

approximation of electric potential, ϕ	number of edges in the element									
	3	4	5	6	7	8	9	10	11	12
linear	0	1	1	1	2	2	2	2	3	3
quadratic	1	2	2	3	3	4	4	4	5	5
cubic	2	3	3	4	4	5	5	6	6	6

in mechanical problems. Hence, even a linear polynomial function in terms of the edge coordinates would suffice to define ϕ along element edges, whereas higher order approximations may also be considered if necessary. While solving electromechanically coupled problems in a numerical framework as the finite element method, an element stiffness matrix $\boldsymbol{K}_e$ will have full rank if the rank requirement conditions for mechanical and electrical parts are satisfied independently, apart from using appropriate integration rules. The rank requirement condition of a mechanical element is defined by Eq. (15) which, in the case of a solely electrical element, turns out to be

$$m \geq i - r \,. \tag{21}$$

In the above equation, m refers to the rank of the element stiffness matrix of a purely electrical element and i to the number of degrees of freedom of the element. With ϕ being the only degree of freedom per node, i equals the number of nodes of the element. As there is one constant electric potential in a plane electrical element, r takes the value of one. As detailed in section 3 for mechanical cases, the rank of $\boldsymbol{K}_e$ for electrical elements depends not only on the number of nodes in the polygonal element but also on the choice of approximation function of $\boldsymbol{D}$ – to be specific, on the number of columns in $\boldsymbol{M}_D$. Hence, consistent with Eq. (21) and also for the completeness of the polynomial functions, it has been suggested to use different higher order approximation functions depending on the number of edges in the polygonal element, as well as on the order of approximation of ϕ to make every individual $\boldsymbol{K}_e$ rank sufficient as indicated in Tab. 5 (Sze and Sheng, 2005). However, it is proposed here to fix the order of $\boldsymbol{M}_D$ for all polygonal elements – in view of boundary value problems discretised with randomly generated Voronoi based meshes – only based on the approximation order of ϕ and not on the number of edges of the element. This is consistent with our suggestion for polynomial approximation functions for stresses in section 3. Thus, while combining the PolyFEM with random Voronoi based discretisations to solve electromechani-

cally coupled problems, the order of $\boldsymbol{M}_\sigma$ and $\boldsymbol{M}_D$ can be chosen only based on the order of approximation functions of $\boldsymbol{u}$ and ϕ and not based on Tab. 1 and Tab. 5. This will obviously result in many of the individual element stiffness matrices to be rank insufficient. However, the so-thought unique property of the Voronoi based discretisations enables the global stiffness matrices to be of full rank after the essential boundary conditions are enforced. This is demonstrated by some examples in the following section.

4.1 Numerical examples

A 1×1 mm^2 piezoelectric plane domain is discretised with the same Voronoi based polygonal meshes that are used for the purely mechanical problems in section 3.1. Homogeneous material properties are assigned to all polygonal elements. Under plane strain conditions, the elastic, piezoelectric and dielectric terms defined in Eq. (3) are expressed as

$$\boldsymbol{s}_{\mathrm{v}} = \begin{bmatrix} s_{11} & s_{13} & 0 \\ s_{13} & s_{33} & 0 \\ 0 & 0 & s_{44} \end{bmatrix}; \quad \boldsymbol{e}_{\mathrm{v}}^{\mathrm{t}} = \begin{bmatrix} 0 & e_{31} \\ 0 & e_{33} \\ e_{15} & 0 \end{bmatrix}; \quad \boldsymbol{h} = \begin{bmatrix} h_{11} & 0 \\ 0 & h_{33} \end{bmatrix} \tag{22}$$

where s_{11} = 139; s_{13} = 74.3; s_{33} = 113; s_{44} = 25.6 GPa, e_{15} = 13.44; e_{31} = -6.98; e_{33} = 13.84 C/m^2 and h_{11} = 6; h_{33} = 5.47 C/GV/m; compare (Park and Sun, 1995).

4.1.1 Piezoelectric response under tension

A tensile load is applied to the piezoelectric domain of interest along the x-axis as the poling direction of the material is considered to coincide with the z-axis. In addition to the mechanical boundary conditions from Fig. 1(a) and (b), the following electrical boundary conditions are enforced on the piezoelectric domain

$$\begin{aligned} &\phi = 0 \quad \text{at} \quad z = 0\,, \\ &\bar{w} = 0 \quad \text{at} \quad z = h\,, \\ &\bar{w} = 0 \quad \text{at} \quad x = 0 \quad \text{and} \quad x = l\,. \end{aligned} \tag{23}$$

The analytical solution of tensile loading on a piezoelectric specimen under plane strain conditions can easily be derived based on the coordinate system specified in Fig. 1 as

$$u_x = c_{11}\,\mathrm{T}\,x\,, \qquad u_z = c_{13}\,\mathrm{T}\,[z - \tfrac{1}{2}h]\,, \qquad \phi = g_{31}\,\mathrm{T}\,z\,, \tag{24}$$

where $c_{11} = 7.9218 \times 10^{-12}$ m^2/N, $c_{13} = -3.03 \times 10^{-12}$ m^2/N and $g_{31} = -1.7778 \times 10^{-2}$ m^2/C. These values are determined by inverting the electromechanical stiffness matrix $\boldsymbol{S}$. While solving the above coupled problem within the

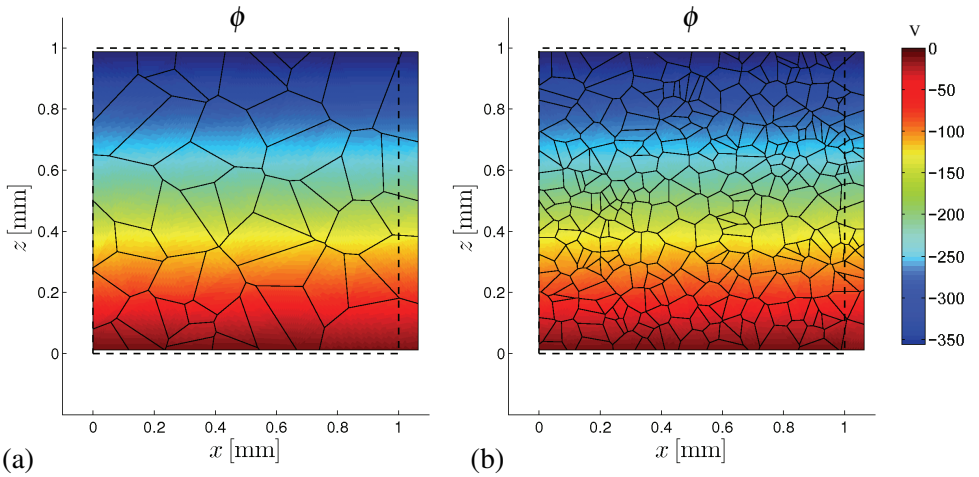

Figure 5: Distribution of the electric potential ϕ for discretisations of (a) 50 and (b) 300 polygonal finite elements under tension, T = 20 MPa. While linear polynomial functions approximate displacements and electric potential along the element edges, $\boldsymbol{M}^1_\sigma$ and $\boldsymbol{M}^1_D$ are employed for the approximation of the stresses and the electric displacements for all polygonal elements irrespective of their number of edges.

PolyFEM, $\boldsymbol{u}$ and ϕ are linearly approximated along the element edges. Without considering the stress and electric displacement approximation functions from Tab. 1 and Tab. 5, $\boldsymbol{M}^1_\sigma$ and $\boldsymbol{M}^1_D$ are employed in all polygonal elements regardless of the number of edges of each element. The global stiffness matrix turned out to possess full rank for all types of Voronoi meshes and the exact solutions are produced. A comparison between the analytical and PolyFEM solutions at points A, B and C is presented in Tab. 6 for $\boldsymbol{u}$ and ϕ for T = 20 MPa. The distribution of ϕ, as determined by the PolyFEM, on the discretisations of 50 and 300 polygonal finite elements is shown in Fig. 5 which is also consistent with the analytical solution.

4.1.2 Piezoelectric response under bending

Now, a pure bending case for the piezoelectric domain is considered to ascertain the specific properties of the random Voronoi based discretisations. Retaining the mechanical boundary conditions from Fig. 1(a) and (c), the following electrical boundary conditions are also enforced to achieve the bending loading,

$$\begin{aligned} &\phi = 0 \quad \text{at} \quad z = 0 \quad \text{and} \quad z = h\,, \\ &\bar{w} = 0 \quad \text{at} \quad x = 0 \quad \text{and} \quad x = l\,, \end{aligned} \tag{25}$$

Table 6: Comparison of the displacements (in μm) and the electric potential (in V) between the analytical and the PolyFEM solution for the piezoelectric domain loaded under tension.

	point A		point B		point C	
	analytical	PolyFEM	analytical	PolyFEM	analytical	PolyFEM
u_x	0.1584	0.1584	0.1584	0.1584	0.1584	0.1584
u_z	0.0303	0.0303	0	0.0000	-0.0303	-0.0303
ϕ	0	0	-177.7838	-177.7838	-355.5677	-355.5677

Table 7: Comparison of the displacements (in μm) and the electric potential (in V) between the analytical and the PolyFEM solution for a piezoelectric bending case.

	point A		point B		point C	
	analytical	PolyFEM	analytical	PolyFEM	analytical	PolyFEM
u_x	-0.1584	-0.1584	0	0.0000	0.1584	0.1584
u_z	-0.1736	-0.1736	-0.1584	-0.1584	-0.1736	-0.1736
ϕ	0	0	88.8919	88.8919	0	0

for which the analytical solutions, based on the specified $x-z$ coordinate system, can be derived as

$$u_x = 2\,c_{11}\,\mathrm{T}\,x\,[z-\tfrac{1}{2}h]\,, \qquad u_z = c_{13}\,\mathrm{T}\,[z-\tfrac{1}{2}h]^2 - c_{11}\,\mathrm{T}\,x^2\,, \tag{26a}$$

$$\phi = g_{31}\,\mathrm{T}\left[(z-\tfrac{1}{2}h)^2 - \tfrac{1}{4}h^2\right]\,. \tag{26b}$$

To solve the above problem with the PolyFEM, quadratic approximations for $\boldsymbol{u}$ and ϕ are used along the element edges, and $\boldsymbol{M}^2_\sigma$ and $\boldsymbol{M}^2_D$ are employed in all polygonal elements. As seen in the previous cases, many of the individual $\boldsymbol{K}_e$ possess rank deficiencies. The global stiffness matrix, however, always turns out to be rank sufficient after applying the essential boundary conditions. Exact solutions are reproduced for all types of discretisations considered and a comparison with the analytical solutions is provided in Tab. 7 for T = 20 MPa/mm. The distributions of σ_{xx} and ϕ for a discretisation with 200 polygonal finite elements are also highlighted in Fig. 6. The results are consistent with the exact solutions. The same results are reproduced by all types of meshes, while using $\boldsymbol{M}^3_\sigma$ and $\boldsymbol{M}^3_D$ for all polygonal elements along with cubic approximations of $\boldsymbol{u}$ and ϕ. Nevertheless, for the same cubic approximations of $\boldsymbol{u}$ and ϕ, the use of polynomial functions for $\boldsymbol{\sigma}$ and $\boldsymbol{D}$ with an order less than two results in rank deficient global stiffness matrices for all six meshes. As seen for the mechanical cases, the relation between the approximation functions of the electromechanical fluxes ($\boldsymbol{\sigma}$ and $\boldsymbol{D}$) and the electromechanical degrees of freedom ($\boldsymbol{u}$ and ϕ) appears to hold for the meshes generated by random

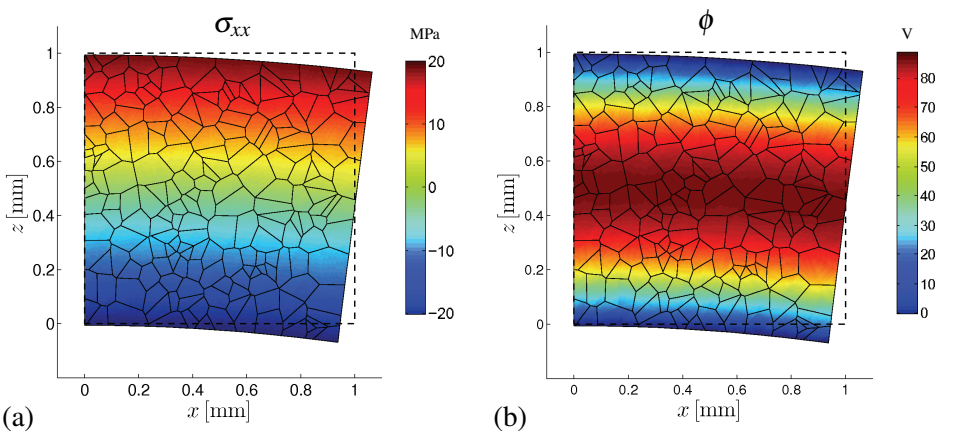

Figure 6: Distributions of (a) σ_{xx} and (b) ϕ are visualised on the piezoelectric domain discretised by 200 polygonal elements for the pure bending case. While quadratic polynomial functions approximated the displacements and electric potential along the element edges, only $\boldsymbol{M}_{\sigma}^{2}$ and $\boldsymbol{M}_{D}^{2}$ were employed for the approximation of the stresses and electric displacements respectively in all elements.

Voronoi based discretisations. To give an example, when the piezoelectric domain is discretised by meshes with regular polygons like square or rectangular elements, the use of $\boldsymbol{M}_{\sigma}^{2}$ and $\boldsymbol{M}_{D}^{2}$ for all elements along with quadratic approximations of $\boldsymbol{u}$ and ϕ resulted in rank deficient global stiffness matrices for all meshes. Similarly, while using $\boldsymbol{M}_{\sigma}^{3}$ and $\boldsymbol{M}_{D}^{3}$ along with cubic approximations of $\boldsymbol{u}$ and ϕ in these regular meshes, the global element stiffness matrices turned out rank insufficient. For meshes different from the naturally evolving or rather the random Voronoi based discretisations, the order of polynomial approximation functions for the stresses and the electric displacements should be chosen from Tab. 1 and Tab. 5.

5 Application of the PolyFEM to a piezoceramic microstructure

Homogeneous material properties were assigned to the discretisations studied in sections 3 and 4, since the main focus was to investigate a patch-test type behaviour of the polygonal finite element examples; similar to the ones applied to the standard finite elements (Taylor, Simo, Zienkiewicz, and Chan, 1986). On the other hand, mesoscopic or micromechanical modelling includes, in addition to other effects such as the switching phenomena, intergranular effects arising from the crystallographic orientation mismatch between neighbouring grains. Piezoceramics or

rather ferroelectrics of ABO_3 crystal structure possess a microstructure wherein the strains, as well as the polarisations vary in different grains. These ferroelectrics are widely used as piezoelectric materials after poling – a process during which a strong electric field is applied onto the specimen to transform it from a ferroelectric to a piezoelectric material. During this process, most of the underlying unit cells or rather crystal variants with similar spontaneous polarisations, also called domains, align their polarisation directions according to the poling axis. This polarisation reorientation process is called domain switching (Jaffe, Cook, and Jaffe, 1971). After poling, the spontaneous polarisation of all variants in piezoceramics, from a modelling point of view, may be considered to fall within a 45° cone, the central axis of which is aligned with the poling axis (Kamlah, 2001). In this context, we assume that the average polarisation of a grain in a poled piezoceramic will be oriented close to the poling axis within certain bounds. For piezoceramics of tetragonal crystal structure, this bound can reasonably be considered to be within the range of $\pm 45°$. The material properties of piezoceramic grains can then be assigned based on their average polarisation directions. Thus, each grain will differ from its neighbouring ones in terms of the averaged strains and polarisations and also in terms of the material properties. The corresponding mismatch or rather intergranular effects can directly be addressed by the PolyFEM.

To represent such a poled piezoceramic microstructure in the simulations, the two-dimensional plane specimen is discretised with random Voronoi based polygons, and each polygonal element is considered to represent a single piezoelectric grain. Treating the z-axis as the poling axis, randomly generated orientations within $\pm 45°$ to the z-axis are assigned to the grains or rather elements to denote the average polarisation directions. Eq. (22) provides the material properties directly for the elements whose average polarisations align with the z-axis. For other elements, the material properties are assigned after appropriate transformations; refer Jayabal, Arockiarajan, and Sivakumar (2008); Menzel, Arockiarajan, and Sivakumar (2008). Thus, the heterogeneity of the poled piezoceramic microstructure, i.e. the randomness in the grain geometries and in the material properties, are realised in a way to realistically represent the material's microstructure. While applying the PolyFEM to such a poled piezoceramic microstructure, linear approximations on $\boldsymbol{u}$ and ϕ are introduced along the element edges. To define the stresses and electric displacements within the elements, $\boldsymbol{M}_{\sigma}^{1}$ and $\boldsymbol{M}_{D}^{1}$ are employed in all polygonal elements. A tensile load of T = 20 MPa is applied on the discretisation of the poled piezoceramic using the same boundary conditions detailed in section 4.1.1. The distribution of σ_{xx} and E_z across the discretisation with 100 polygonal finite elements is shown in Fig. 7(a) and (b). As highlighted in the contour plots, the maximum values of σ_{xx} reach up to 24 MPa and E_z approaches 0.5 MV/m. For the same load-

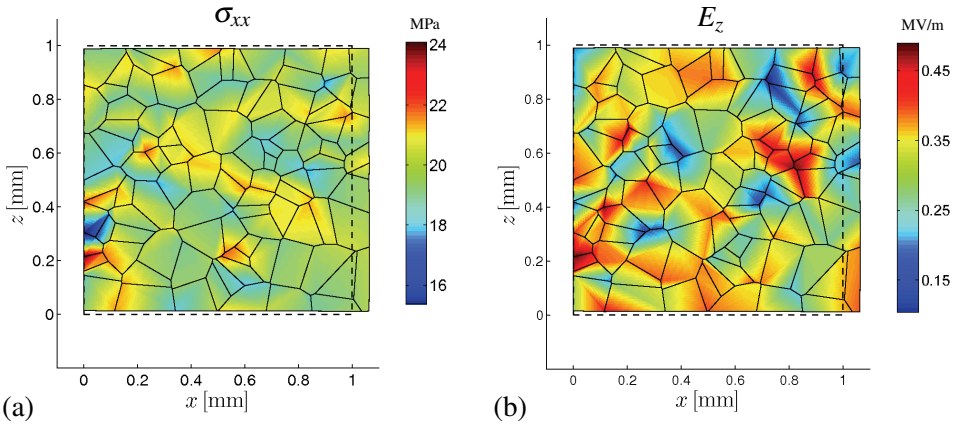

Figure 7: Distribution of (a) σ_{xx} and (b) E_z for a discretisation with 100 Voronoi polygonal finite elements corresponding to a representative microstructure of a poled piezoceramic. Due to the intergranular effects and different crystallographic orientations, the values of the stress and electric field increase in some regions which, in general, can cause localised domain switching in the material.

ing conditions, σ_{xx} and E_z remain constant throughout the material at 20 MPa and 0.3556 MV/m respectively in section 4, where homogeneous material properties are used. Higher magnitudes of stresses and electric fields, beyond their coercive values, induce domain switching in piezoceramics resulting in modifications of macroscopic material properties (Jaffe, Cook, and Jaffe, 1971; Lynch, 1996). This would, in turn, affect the performance of the devices employing the piezoceramic specimens. Hence, while designing piezo devices, especially of small length scales, these localised higher magnitudes of stresses and electric fields are important and influence the long-life properties of the device. Within the approach discussed in this work, the naturally evolving irregular polygons of Voronoi discretisations reasonably resemble the grain geometry – definitely better than discretisations where one quadrilateral or regular hexagon represents one grain – whereas their material properties correspond to that of a poled piezoceramic. Such a representation combines the advantages of both micro and macro modelling aspects – bringing additional insight of the microstructure into an efficient numerical framework while keeping the computational cost reasonably low.

6 Summary

In this work, a specific advantage of employing a hybrid finite element approach on random Voronoi based discretisations is identified. Accordingly, contrary to the conditions imposed in the literature that different higher order approximation functions would be required in mechanical problems to approximate stresses within the polygonal finite elements based on the number of element edges, it is proposed here to use the same approximation function in all elements. Also, the order of polynomial approximation function for the stresses can be chosen based on the order of approximation functions defining the displacements along the element edges and not related to the number of edges of the polygonal elements. To be more specific, the order of the stress approximation function can be chosen of equal order as that of the approximation function for the displacements. By analogy with purely mechanical problems, the approximation function for the electric displacements can be chosen based only on the order of approximation function of electric potential along the element edges. Although this procedure may cause many of the individual element stiffness matrices to become rank insufficient, the global stiffness matrix always turned out to possess full rank on enforcing the essential boundary conditions. This is demonstrated in this work by means of several representative examples. Some of the examples are set up by analogy with standard patch tests and were performed for different Voronoi based polygonal discretisations. The relation is expected to hold for any randomly generated Voronoi polygonal mesh. Once more, it is emphasised that the above relation holds only for naturally evolving or rather random Voronoi based discretisations and not for the special case of Voronoi meshes with, for instance, regular polygons like square or rectangular elements. The conclusion from this work is to save considerable computational costs when simulating boundary value problems with the PolyFEM, as the polynomial degree for the approximation chosen can be reduced. This makes the application of the PolyFEM to simulations of polycrystalline microstructures even more efficient which becomes of cardinal importance for nonlinear boundary value problems.

References

Aurenhammer, F. (1991): Voronoi diagrams – a survey of a fundamental geometric structure. *AMC Computing Surveys*, vol. 23, pp. 345–405.

Braess, D. (2001): *Finite Elements. Theory, fast solvers, and applications in solid mechanics*. Cambridge University Press, 2nd edition.

Brezzi, F.; Fortin, M. (1991): *Mixed and Hybrid Finite Element Methods*. Springer-Verlag, Berlin – Heidelberg – New York.

Ghosh, S.; Mallett, R. L. (1994): Voronoi cell finite elements. *Computers & Structures*, vol. 50, pp. 33–46.

Ghosh, S.; Moorthy, S. (1995): Elastic-plastic analysis of arbitrary heterogeneous materials with the Voronoi cell finite element method. *Computer Methods in Applied Mechanics and Engineering*, vol. 121, pp. 373–409.

Haug, A.; Huber, J. E.; Onck, P. R.; Van der Giessen, E. (2007): Multi-grain analysis versus self-consistent estimates of ferroelectric polycrystals. *Journal of the Mechanics and Physics of Solids*, vol. 55, pp. 648–665.

Jaffe, B.; Cook, W. R.; Jaffe, H. (1971): Piezoelectric ceramics. *Academic Press, London*.

Jayabal, K.; Arockiarajan, A.; Sivakumar, S. M. (2008): A micromechanical model for polycrystal ferroelectrics with grain boundary effects. *CMES: Computer Modeling in Engineering & Sciences*, vol. 27, pp. 111–123.

Kamlah, M. (2001): Ferroelectric and ferroelastic piezoceramics - modeling and electromechanical hysteresis phenomena. *Continuum Mechanics and Thermodynamics*, vol. 13, pp. 219–268.

Kamlah, M.; Liskowsky, A. C.; McMeeking, R. M.; Balke, H. (2005): Finite element simulation of a polycrystalline ferroelectric based on a multidomain single crystal switching model. *International Journal of Solids and Structures*, vol. 42, pp. 2949–2964.

Kim, S. J.; Jiang, Q. (2002): A finite element model for rate-dependent behavior of ferroelectric ceramics. *International Journal of Solids and Structures*, vol. 39, pp. 1015–1030.

Landis, C. M. (2002): A new finite-element formulation for electromechanical boundary value problems. *International Journal for Numerical Methods in Engineering*, vol. 55, pp. 613–628.

Lynch, C. (1996): The effect of uniaxial stress on the electro-mechanical response of 8/65/35 PLZT. *Acta Materialia*, vol. 44, pp. 4137–4148.

Menzel, A.; Arockiarajan, A.; Sivakumar, S. M. (2008): Two models to simulate rate-dependent domain switching effects–application to ferroelastic polycrystalline ceramics. *Smart Materials and Structures*, vol. 17, pp. 15026–38.

Nye, J. F. (1985): *Physical Properties of Crystals – Their Representation by Tensors and Matrices*. Oxford Science Publications.

Oden, J. T.; Carey, G. F. (1983): *Finite Elements. Mathematical Aspects*, volume IV. Prentice-Hall, Englewood Cliffs, New Jersey.

Park, S. B.; Sun, C. T. (1995): Effect of electric field on fracture of piezoelectric ceramics. *International Journal of Fracture*, vol. 70, pp. 203–216.

Pian, T. H. H. (1964): Derivation of element stiffness matrices by assumed stress distribution. *American Institute of Aeronautics and Astronautics*, vol. 2, pp. 1333–1336.

Sze, K. Y.; Sheng, N. (2005): Polygonal finite element method for nonlinear constitutive modeling of polycrystalline ferroelectrics. *Finite Elements in Analysis and Design*, vol. 42, pp. 107–129.

Taylor, R. L.; Simo, J. C.; Zienkiewicz, O. C.; Chan, A. C. H. (1986): The patch test – a condition for assessing FEM convergence. *International Journal for Numerical Methods in Engineering*, vol. 22, pp. 39–62.

Timoshenko, S. P.; Goodier, J. N. (1970): *Theory of Elasticity*. Third Edition, McGraw-Hill Publications.